HHS Public Access

Author manuscript

*Mol Cancer Ther*. Author manuscript; available in PMC 2022 June 01.

Published in final edited form as:

*Mol Cancer Ther*. 2021 June ; 20(6): 975–985. doi:10.1158/1535-7163.MCT-20-0462.

# The KRAS$^{G12C}$ Inhibitor MRTX849 Reconditions the Tumor Immune Microenvironment and Sensitizes Tumors to Checkpoint Inhibitor Therapy

**David M. Briere**[1], **Shuai Li**[2], **Andrew Calinisan**[1], **Niranjan Sudhakar**[1], **Ruth Aranda**[1], **Lauren Hargis**[1], **David H. Peng**[2], **Jiehui Deng**[2], **Lars D. Engstrom**[1], **Jill Hallin**[1], **Sole Gatto**[3], **Julio Fernandez-Banet**[3], **Adam Pavlicek**[3], **Kwok-Kin Wong**[2], **James G. Christensen**[1], **Peter Olson**[1]

[1]Mirati Therapeutics, Inc., San Diego, California.

[2]Laura and Isaac Perlmutter Cancer Center, New York University School of Medicine, NYU Langone Health, New York City, New York.

[3]Monoceros Biosystems LLC, San Diego, California.

## Abstract

KRAS$^{G12C}$ inhibitors, including MRTX849, are promising treatment options for KRAS-mutant non–small cell lung cancer (NSCLC). PD-1 inhibitors are approved in NSCLC; however, strategies to enhance checkpoint inhibitor therapy (CIT) are needed. *KRAS$^{G12C}$* mutations are smoking-associated transversion mutations associated with high tumor mutation burden, PD-L1 positivity, and an immunosuppressive tumor microenvironment. To evaluate the potential of MRTX849 to augment CIT, its impact on immune signaling and response to CIT was evaluated. In human tumor xenograft models, MRTX849 increased MHC class I protein expression and



**Corresponding Author:** Peter Olson, Mirati Therapeutics, Inc., San Diego, CA 92121. Phone: 1 (858) 332-3554; olsonp@mirati.com.

Authors' Contributions

**D.M. Briere:** Conceptualization, resources, supervision, investigation, methodology, project administration, writing–review and editing. **S. Li:** Conceptualization, resources, formal analysis, supervision, investigation, methodology. **A. Calinisan:** Formal analysis, investigation. **N. Sudhakar:** Formal analysis, investigation. **R. Aranda:** Formal analysis, investigation. **L. Hargis:** Formal analysis, investigation. **D.H. Peng:** Formal analysis, investigation. **J. Deng:** Formal analysis, investigation. **L.D. Engstrom:** Supervision, investigation. **J. Hallin:** Supervision, investigation. **S. Gatto:** Formal analysis, investigation, methodology. **J. Fernandez-Banet:** Formal analysis, supervision, investigation, methodology. **A. Pavlicek:** Formal analysis, supervision, validation, methodology. **K.-K. Wong:** Conceptualization, supervision, funding acquisition, investigation, methodology, project administration. **J.G. Christensen:** Conceptualization, resources, supervision, investigation, writing–review and editing. **P. Olson:** Conceptualization, formal analysis, supervision, investigation, methodology, project administration.

Authors' Disclosures

D.M. Briere reports a patent for 62/905,107 pending. A. Calinisan reports personal fees from Mirati Therapeutics during the conduct of the study; personal fees from Mirati Therapeutics outside the submitted work; and is an employee of Mirati Therapeutics. N. Sudhakar reports other support from Mirati Therapeutics outside the submitted work. R. Aranda reports other support from Mirati Therapeutics outside the submitted work. A. Pavlicek is a shareholder of Mirati Therapeutics. K.-K. Wong reports grants from Mirati during the conduct of the study; other support from G1 Therapeutics and Zentalis outside the submitted work. J.G. Christensen reports personal fees from Mirati Therapeutics during the conduct of the study; in addition, J.G. Christensen has a patent for Mirati Therapeutics issued. P. Olson reports other support from Mirati Therapeutics during the conduct of the study and has a patent for PCT/US20/52185 pending to Mirati Therapeutics. No disclosures were reported by the other authors.

**Note:** Supplementary data for this article are available at Molecular Cancer Therapeutics Online (http://mct.aacrjournals.org/).

decreased RNA and/or plasma protein levels of immunosuppressive factors. In a *Kras*$^{G12C}$-mutant CT26 syngeneic mouse model, MRTX849 decreased intratumoral myeloid-derived suppressor cells and increased M1-polarized macrophages, dendritic cells, CD4$^{+}$, and CD8$^{+}$ T cells. Similar results were observed in lung *Kras*$^{G12C}$-mutant syngeneic and a genetically engineered mouse (GEM) model. In the CT26 *Kras*$^{G12C}$ model, MRTX849 demonstrated marked tumor regression when tumors were established in immune-competent BALB/c mice; however, the effect was diminished when tumors were grown in T-cell–deficient *nu/nu* mice. Tumors progressed following anti–PD-1 or MRTX849 single-agent treatment in immune-competent mice; however, combination treatment demonstrated durable, complete responses (CRs). Tumors did not reestablish in the same mice that exhibited durable CRs when rechallenged with tumor cell inoculum, demonstrating these mice developed adaptive antitumor immunity. In a GEM model, treatment with MRTX849 plus anti–PD-1 led to increased progression-free survival compared with either single agent alone. These data demonstrate KRAS inhibition reverses an immunosuppressive tumor microenvironment and sensitizes tumors to CIT through multiple mechanisms.

## Introduction

The discovery of clinically active KRAS$^{G12C}$ inhibitors provides a much-needed targeted therapy for patients with this mutation (1, 2). *KRAS*$^{G12C}$ mutations are present in approximately 14% of non–small cell lung cancer (NSCLC), approximately 4% of colorectal cancer and several other cancers at lower frequency. The treatment paradigm for several cancers has recently been transformed by checkpoint inhibitor therapy (CIT) targeting the PD-1/PD-L1 pathway which now constitutes a front-line treatment option as a single agent or in combination with chemotherapy and/or other therapies in NSCLC (3-6). In NSCLC, initial data demonstrated single-agent CIT was effective and durable; however, only in a subset of patients, which triggered a major effort to identify patients most likely to respond and to identify combinations with increased activity.

*KRAS*$^{G12C}$ mutations are smoking-induced transversion mutations found in tumors with high tumor mutation burden (TMB), a genomic biomarker associated with increased response to CIT (7, 8). Mutant *KRAS* is linked to PD-L1 expression and oncogenic RAS signaling promotes immune resistance by upregulating PD-L1 expression (9). Available clinical data suggest CIT is effective in *KRAS*-mutant NSCLC; however, additional strategies are needed to improve the activity of this therapeutic modality (10, 11). These data highlight the molecular features and tumor-immune biology driven by *KRAS*$^{G12C}$ mutations in NSCLC and suggest inhibition of KRAS may work together with PD-1–targeted therapy to improve activity of either single agent.

Although combinations involving CIT plus targeted therapies against other oncogenic drivers have not been successful in the clinic to date, there is strong biological rationale to suggest KRAS inhibition may complement CIT when utilized in combination. Studies conducted in GEM models exhibiting spontaneous tumors driven by mutated KRAS demonstrated oncogenic KRAS orchestrates an immunosuppressive tumor microenvironment and is responsible for CIT resistance (12, 13). In these models, KRAS activation leads to the increased secretion of IL23, CCL9, VEGFA, and CXCL3 by tumor

cells which recruits immunosuppressive macrophages and myeloid-derived suppressor cells (MDSC) into the tumor microenvironment resulting in the exclusion of adaptive T and B cells in a PD-L1–dependent manner. Resistance to anti–PD-1 therapy in *KRAS*-mutant tumors was overcome through inhibition of downstream KRAS signaling through the IRF2 and Myc pathways (12, 13). The regulation of VEGF by RAS has been primarily characterized as a mechanism to upregulate tumor angiogenesis (14-16). However, the ability of VEGF to regulate immune suppression via recruitment of immature dendritic cells and MDSCs is another mechanism of tumor promotion and the VEGF pathway is currently being targeted for the treatment of several cancers, including in combination with CIT (17-19). The regulation of the cytokines IL6 and IL8 by RAS further contribute to angiogenesis and an aggressive phenotype via paracrine signaling (20, 21). Blocking oncogenic RAS was also shown to enhance tumor cell surface expression of MHC class I expression (22). Reexpression of antigen presentation machinery is likely required to elicit a maximal antitumor immune response.

In this study, various mouse models were used to elucidate the molecular and cellular effects of $KRAS^{G12C}$ inhibition on tumor and immune biology. These data demonstrate inhibition of $KRAS^{G12C}$ indeed reverses immunosuppressive signaling through regulation of key immune signaling factors, and, in addition, induces dramatic reconditioning of the tumor immune microenvironment. Importantly, $KRAS^{G12C}$ inhibition and anti–PD-1 therapy induced durable tumor regressions and endowed animals with antitumor immunity, providing strong rationale to test this combination clinically.

## Material and Methods

### Compounds and reagents

MRTX849 was synthesized at WuXi AppTec (lot No. EW5243-1094-P1). MRTX849 in powder form was stored at room temperature and protected from light. MRTX849 was formulated at 100 mg/kg with 10% Captisol (Cydex Pharmaceuticals lot No. NC-04A-180185) in 50 mmol/L citrate buffer pH 5.0 once per week and the dosing solution was stored at 4°C protected from light. MRTX849 was administered by oral gavage (orally) daily.

Anti-mouse PD-1 antibody antagonist clone 29F.1A12 (catalog No. BP0273, lot No. 737319J2) and the isotype control antibody, rat IgG2a (catalog No. BP0089, lot No. 686318F1B) were obtained from Bio X Cell. Both reagents were diluted in *In Vivo*Pure Dilution Buffer pH 7.0 (catalog No. IP0070, lot No. 708919F1) obtained from Bio X Cell and administered at 10 mg/kg. Dosing solutions were made fresh for each dose. Both the anti-mouse PD-1 antibody and the rat IgG2a isotype control antibody was administered intraperitoneally.

The CT26.WT (CT26) cell line (ATCC CRL-2638) was maintained *in vitro* with RPMI1640 medium (No. 11875-093), penicillin/streptomycin (No. 15070-063), HEPES [(4-(2-hydroxyethyl)-1-piperazineethanesulfonic acid), No. 15630-080], Sodium Pyruvate (No. 11360-070) obtained from Gibco/Thermo Fisher Scientific and FBS obtained from Corning (No. 35-011-CV, Corning) and Nucleus Biologics (1824-001). The LL/2 cell

line (ATCC CRL-1642) was maintained in DMEM and supplemented with FBS. The lab tested for *Mycoplasma* every few months using a commercially available test [MycoAlert Detection kit (Lonza); catalog No. LT07-418). CRISPR-engineered cell lines underwent single-cell cloning therefore cell line clones underwent several passages during scale up and during the course of these studies.

### CRISPR/Cas9 engineering mouse syngeneic *Kras*$^{G12C}$-mutant tumor cell lines

The mouse colon cancer cell line CT26 was genetically modified to express KRAS$^{G12C}$. The CT26 cell line is triallelic for the *Kras* gene and each allele harbors a mutation at codon 12 that changes a glycine residue (G) to an aspartic acid residue (D; ref. 23). To create a CT26 cell line derivative harboring the *Kras*$^{G12C}$ mutation, the G12D codon was changed to a G12C codon using a Clustered Regularly Interspaced Short Palindromic Repeats/CRISPR-associated 9 (CRISPR/Cas9) system (Synthego) in the following manner. A synthetically modified single-guide ribonucleic acid (sgRNA) targeting the region near the *Kras* 12 codon was designed and synthesized on the basis of high specificity and propensity to create double strand breaks when complexed with the Cas9 DNA endonuclease. A single-stranded oligodeoxynucleotide (ssODN) was designed to enable homologous donor repair at the site of the sgRNA cut site and introduce the desired cysteine codon (GAT: D to TGT: C) at position 12 while also introducing silent mutations to prevent recutting. Cas9/sgRNA riboprotein complexes and ssODN were transfected into CT26 cells. sgRNA and ssODN sequences are provided in Supplementary Data. Single-cell CT26 clones were isolated, and their genotypes were screened by Sanger DNA sequencing and Inference of CRISPR Edits (ICE) analysis (Synthego) to identify homozygous G12C-targeted clones. The CT26 *Kras*$^{G12C}$ E3 clone was selected for *in vivo* studies.

The mouse lung cancer cell line LL/2 harbors *Kras*$^{G12C}$ and *Nras*$^{Q61H}$ mutations and was genetically modified to no longer express functional *Nras*. *Nras*-targeting sgRNAs complexed with Cas9 protein were transfected into LL/2 cells and single-cell clones were grown up and screened to identify clones that harbored inactivating mutations in *Nras*.

### Immunoblotting

Cells and tumors were lysed with either RIPA (Thermo Fisher Scientific, No. 8990) or Lysis/Binding Buffer AM11 (Active Motif, No. 52097) with protease and phosphatase inhibitors added fresh before use. Cells in 10-cm plates were treated as described previously, or tumor fragments were snap frozen in homogenization tubes (Omni, No. 19-628-3) after treatment as described previously. Tumor fragments were lysed with approximately 500-μL lysis buffer added and homogenized with three rounds of shaking, 20 seconds each, on ice (MPBio, FastPrep-24 system). Cell pellets were collected by scraping on ice with PBS with protease and phosphatase inhibitors before transferring to a 1.5-mL microcentrifuge tube and spun in a centrifuge at 14,000 × *g* for 20 seconds at 4°C. Cell pellets were then snap frozen on dry ice before lysing with lysis buffer. Cell lysates were left on ice for 30 minutes and vortexed four times to ensure complete lysis. Cell and tumor lysates were spun in a centrifuge at 14,000 × *g* for 15 minutes at 4°C. All sample supernatants were stored at −80°C. For immunoblotting, 30 μg of protein were loaded onto a 12% Bis-Tris gel (Bio-Rad, No. 3450118) and run according to manufacturer instructions with the Precision

Plus Protein Kaleidoscope Prestained Protein Standards (Bio-Rad, No. 1610375). Proteins were transferred onto Nitrocellulose membrane (Life Technologies, No. IB23001) using the IBlot Dry Blotting system (Life Technologies). Primary antibodies were added overnight at 4°C with rocking. KRAS antibody was purchased from Sigma-Aldrich (product No. SAB1404011). pERK (9101L), pS6 (2211L), ERK (9102L), S6 (2217L), and Alpha tubulin (3873S) antibodies were purchased from Cell Signaling Technology. The next day, the primary antibodies were removed, blots were washed five times with 1× TBS + 0.1% Tween-20, and solutions consisting of LI-COR IRDye secondary antibodies were added for 2 hours at room temperature with shaking. After secondary incubation, the wells were washed again and imaged using the LI-COR Odyssey CLx Imaging system (LI-COR) set to the AutoScan channel for both the 700 and 800 wavelength channels to measure the signal intensity from the IRDye 680RD goat anti-rabbit and IRDye 800CW goat anti-mouse secondary antibodies, respectively. Images were imported into LiCor's Image Studio software version 4.0 and then .tif files were exported to Windows Photo Viewer.

### Cell proliferation assays

Cells were plated in 96-well white-walled plates (No. 3917, Corning) for cell viability determination in standard tissue culture conditions. The day after plating, serial dilutions of MRTX849 to evaluate a concentration-dependent effect on cell viability were made using Rainin multichannel pipettes. A total of 72 hours later, the CellTiter-Glo Luminescent Cell Viability Assay (No. G7573, Promega) was used to measure cell viability effects of MRTX849. Plates were read where luminescence was measured using a ClarioStar plate reader (BMG Labtech). Data were analyzed and $IC_{50}$ values were determined using GraphPad Prism (GraphPad). Viable cells were counted at the beginning of the assay using a Cellometer Mini (Nexcelom Bioscience) using Trypan Blue exclusion so as to plate the same number of viable cells per well at the beginning of the experiment.

### Generation and therapeutic treatment of *Kras$^{G12C}$*-mutant genetically engineered mouse models

All genetically engineered mouse model (GEMM) studies, including breeding and treatment studies, were performed with approval of the Institutional Animal Care and Use Committee (IACUC) at New York University School of Medicine (New York City, NY). The GEM harbors a conditional activating mutation of h*KRAS$^{G12C}$* at the collagen I locus (Li and colleagues, 2018). *p53*$^{R270H}$ (mutant omologous to human p53$^{R273H}$) and Msh2$^{tm2.1Rak}$ (MSH2 deletions for studying DNA mismatch repair) were obtained from The Jackson laboratory. CRE recombinase was induced in 6-week-old littermates through intranasal inhalation of $2.5 \times 10^6$ pfu adeno-Cre (University of Iowa adenoviral core) for LSL-*KRAS$^{G12C}$ Trp53$^{R270H}$* GEMM (KCP) and $1 \times 10^7$ pfu for the LSL-*KRAS$^{G12C}$ Msh2$^{fl/f}$* (KCM). Lung adenocarcinoma appeared 6 weeks after induction for KCP, and 12 weeks for KCM. Once MRI showed the tumor size reached 300 to 400 $mm^3$, mice were randomly assigned to treatment groups. No gender bias between male and female mice was observed regarding to the tumor growth and response to drug treatment. Mice were treated with MRTX1257 50 mg/kg once daily by oral gavage, either alone or in combination with anti-PD1 10 mg/kg three times a week by intraperitoneally. Vehicle control and isotype control were included as well. For efficacy studies, GEMMs were dosed with a low dose

of 10 mg/kg MRTX849 and dosed continuously for long term and monitored by MRI every 2 weeks. For immune profiling studies, GEMMs were dosed for 6 days. Progression-free survival (PFS) was analyzed based on the standard criteria in clinical trials. Briefly, PFS was the duration between treatment start and progression, which was defined by increase of tumor size compared with the previous scan of MRI and the appearance of new lesions. Survival data were calculated using Kaplan–Meier log-rank test.

## Syngeneic mouse model studies

All mouse studies were conducted in compliance with all applicable regulations and guidelines of the IACUC from the NIH. Mice were maintained under pathogen-free conditions, and food and water were provided *ad libitum*. Eight- to 10-week-old female BALB/c mice (Envigo) were injected subcutaneously with CT26 $Kras^{G12C}$ tumor cells in 100 μL of PBS and Matrigel matrix (Corning No. 356237; Discovery Labware) in the right hind flank with 1.0e6 cells 50:50 cells: Matrigel. Rechallenge mice were injected subcutaneously with tumor cells in 100 μL of PBS and Matrigel matrix in the left hind flank with 1.0e6 cells 50:50 cells:Matrigel. Six-week-old female C57Bl/6 mice (Charles River Laboratories) were injected subcutaneously with LL/2 $Kras^{G12C}$ cells in 100 μL of PBS and Matrigel matrix (Corning No. 356237; Discovery Labware) in the right hind flank with 1.0e6 cells 50:50 cells:Matrigel. Mouse health was monitored daily, and caliper measurements began when tumors were palpable. Tumor volume measurements were determined utilizing the formula $0.5 \times L \times W^2$ in which $L$ refers to length and $W$ refers to width of each tumor. For the combination efficacy study, when tumors reached an average tumor volume of approximately 220 $mm^3$, mice were randomized into four treatment groups, with 10 mice per treatment group. MRTX849 was administered orally, daily and the PD-1 antibody was administered intraperitoneally, every 3 days for three doses. Both MRTX849 and PD-1 were administered alone and in combination. Control mice were dosed by oral gavage with the Captisol oral vehicle and dosed intraperitoneally with the isotype control antibody, every 3 days for three doses. Tumors were measured three times per week and body weights were measured two times per week. For the pharmacodynamic FACS study, when CT26 $Kras^{G12C}$ tumors reached an average tumor volume between 220 and 730 $mm^3$, mice were randomized into treatment groups, with four mice per group. MRTX849 was administered orally, daily for four or eight doses depending on the treatment group and the PD-1 antibody was administered intraperitoneally, every 3 days for two or three doses depending on the treatment group. Both MRTX849 and PD-1 were administered alone and in combination. Control mice were dosed by oral gavage with the Captisol oral vehicle and dosed intraperitoneally with the isotype control antibody. Tumors were measured at randomization and termination; body weights were measured twice weekly.

## Flow cytometry

Tumors were removed 3 hours after the last dose on day 4 or day 8 and placed into Vitacor (formerly Lifor Solution; Detraxi) then shipped to MI Bioresearch overnight on wet ice and processed using a mouse Tumor Dissociation Kit form Miltenyi Biotec. Ice-cold solid tissues were weighed, minced, and placed into a gentleMACS C Tube containing a dissociation enzyme cocktail in culture medium. The cells were resuspended in cell staining buffer and transferred to a new 96-well plate containing prediluted antibodies. The samples

were incubated for 30 minutes protected from light at 4°C. The cells were resuspended in ice-cold cell staining buffer and acquired on the Attune NxT Acoustic Focusing Cytometer. Antibodies used targeted CD45, CD3, CD4, CD8, PD-1, CD49b/CD335, CD69, CD25, FoxP3, CD11b, Ly-6C, Ly-6G, F4/80, MHCII, CD24, CD206, CD19, CD11c, Absolute Counting Beads, Ki-67 Viability.

For GEMM studies, mice were euthanized after 6 days of dosing, tumors microdissected, and tissues fixed for IHC or dissociated to single-cell suspensions for flow cytometry analysis. Tumors were mechanically separated and enzymatically dissociated with collagenase/DNAase for 30 minutes at 37°C. Cells were filtered through a 70 μm cell strainer and red blood cells were lysed with RBC Lysis Buffer (BioLegend) for 5 minutes at room temperature. Cells were resuspended in PBS/2% FBS/1 mmol/LEDTA staining buffer and incubated with surface staining antibodies for 1 hour at room temperature. Cells were washed with staining buffer and resuspended in Fixation/Permeabilization Buffer (BioLegend) for 30 minutes, washed, and incubated with intracellular staining antibodies in 1 × Permeabilization Buffer (BioLegend) for 1 hour at room temperature. Cells were washed and resuspended with staining buffer, and acquired on the BD LSRII Fortessa Cytometer. Antibodies used targeted CD45, CD3, CD4, CD8, CD44, CD62L, PD-1, TIM-3, FOXP3, CTLA4, Ki67, CD11b, CD11c, Ly-6C, Ly-6G, F4/80, Dx5, CD19, and Zombie Aqua Live/Dead Viability stain.

## Results

### $KRAS^{G12C}$ inhibition modifies tumor cell–intrinsic factors that regulate antigen presentation and an immunosuppressive tumor microenvironment

To determine the effects of $KRAS^{G12C}$ inhibition on expression of key genes implicated in the response to PD-1 inhibition by tumor cells, RNA sequencing (RNA-seq) was performed on bulk tumor and human RNA expression was assessed in five $KRAS^{G12C}$-mutant human xenograft tumor models grown in immune-compromised mice treated with vehicle or 100 mg/kg of MRTX849. In a previous study, repeat dose administration of MRTX849 demonstrated significant tumor growth inhibition in each of these models (2). VEGFA, NT5E, CXCL1, and CXCL8 were significantly downregulated in MRTX849-treated tumors in all five models compared with vehicle-treated tumors following a single or repeat dosing after 6 and 24 hours after last dose (Fig. 1A). In addition, MHC genes including HLA-E, HLA-C, HLA-F, HLA-A and HLA-H were significantly upregulated at one or more timepoints in a subset of models, while CD274 was significantly downregulated in three models. Single or repeat dose administration of MRTX849 also significantly decreased the plasma concentration of IL8 (CXCL8 gene) and CXCL1 protein in mice bearing selected xenograft models (Fig. 1B) demonstrating reduced concentration of key immune signaling molecules in the tumor microenvironment as well as systemic circulation. As MRTX849 is in active clinical development, these circulating factors may represent a noninvasive method of monitoring KRAS inhibition in the clinic. The expression of MHC class I protein levels (MHC class I antibody raised against amino acids 63–362 of human HLA-B) was also increased following MRTX849 treatment in several xenograft models as measured by reverse phase protein array analysis across a panel of models (Fig. 1C; ref. 24). Increased

expression of MHC class I protein expression is predicted to enable recognition of tumor cell antigens by the immune system.

## MRTX849 covalently modifies KRAS$^{G12C}$, inhibits KRAS-dependent signaling, and demonstrates tumor regression in CRISPR/Cas9-engineered CT26 *Kras$^{G12C}$* tumors

To explore the impact of KRAS$^{G12C}$ inhibition by MRTX849 and to interrogate the mechanism of response to treatment in an immune-competent tumor model, the CT26.WT cell line was engineered using CRISPR/Cas9 to replace the endogenous *Kras$^{G12D}$* alleles with *Kras$^{G12C}$* (Supplementary Fig. S1). The KRAS$^{G12C}$ protein in two CT26 *Kras$^{G12C}$* cell clones exhibited an upward shift on a Western blot analysis when treated with 300 nmol/L MRTX849 for 24 hours confirming the KRAS$^{G12C}$ protein was expressed and covalently modified by MRTX849 treatment (Fig. 2A). In a 3-day viability assay, MRTX849 demonstrated growth inhibition of the two CT26 *Kras$^{G12C}$* cell clones with $IC_{50}$ values of 65 and 96 nmol/L compared with parental cells, which were relatively insensitive ($IC_{50}$ = 1.7 μmol/L; Fig. 2B). Clone E3 was selected for further characterization *in vitro* and *in vivo*. Treatment of CT26 *Kras$^{G12C}$* E3 clone cells with 1 μmol/L MRTX849 for 6 or 24 hours *in vitro* correlated with strong inhibition of phosphorylated ERK (pERK, Thr202/Tyr204) and phosphorylated S6 (pS6, Ser235/236) as expected following near complete modification of KRAS$^{G12C}$ (Fig. 2C). To evaluate whether antigen presentation machinery were upregulated following KRAS$^{G12C}$ inhibition, CT26 *Kras$^{G12C}$* cell were treated with 300 nmol/L MRTX849 and H-2Dd surface protein was increased as assessed by flow cytometry (Supplementary Fig. S2A).

CT26 *Kras$^{G12C}$* E3 tumors were grown in immune competent BALB/c mice and dramatic KRAS$^{G12C}$ modification and inhibition of pERK (Thr202/Tyr204) and pS6 (Ser235/236) was observed 6 hours following a single oral dose of 100 mg/kg MRTX849 (Fig. 2D). In repeat dose efficacy studies in immune-competent BALB/c mice, treatment with 100 mg/kg/day MRTX849 led to complete responses and treatment with 30 mg/kg/day led to strong tumor growth inhibition confirming CT26 *Kras$^{G12C}$* tumors were highly dependent on KRAS signaling *in vivo* (Fig. 2E). H-2Dd expression was also upregulated in CT26 *Kras$^{G12C}$* tumors from mice dosed for 4 days with MRTX849 100 mg/kg compared with vehicle treated mice (Supplementary Fig. S2B).

## MRTX849 treatment reconditions the tumor microenvironment in *Kras$^{G12C}$* syngeneic models

To characterize the effects of MRTX849 on tumor immune cell populations, CT26 *Kras$^{G12C}$* tumor-bearing BALB/c mice were treated with vehicle or MRTX849 at 100 mg/kg every day for 4 or 8 days. Intact tumors were dissociated and then analyzed for cells of myeloid and lymphoid lineage using flow cytometry. The relative abundance of intratumoral monocytic and granulocytic myeloid-derived suppressor cells (MDSCs) was decreased whereas the fraction of immune-promoting M1-polarized macrophages was increased in both MRTX849 and MRTX849 plus anti–PD-1–treated tumors compared with vehicle at 4- and/or 8-day time points (Fig. 3A). An increase in antigen-presenting dendritic cells was also observed in MRTX849 and MRTX849 plus anti–PD-1–treated tumors at 4 days. In addition, several intratumoral lymphoid populations of T-cell origin were increased at both

4 and 8 days including $CD3^+$ lymphocytes, $CD4^+$ T cells, $CD4^+$ Th cells, T regulatory cells (Tregs), and natural killer (NK) T cells in MRTX849 and MRTX849 plus anti–PD-1–treated tumors compared with vehicle (Fig. 3B). $CD19^+$ B cells were increased in the MRTX849 groups at 8 days of treatment. $CD8^+$ T cells were also significantly increased by MRTX849 at 4 days and a trend toward increased $CD8^+$ T cells were observed at 8 days and in PD-1 and combination-treated mice from both days. The magnitude of the effects on immune cell populations between MRTX849 single agent and MRTX849 plus anti–PD-1–treated tumors were similar and demonstrate significant immune cell changes following combination treatment appear as mostly driven through blockade of $KRAS^{G12C}$. These data demonstrate mutant $KRAS^{G12C}$ is responsible for actively driving immune suppression and that inhibition of KRAS markedly shifts the immune cell repertoire from an immunosuppressive state toward an antitumor immune supportive response.

To evaluate the effect of $KRAS^{G12C}$ inhibition on immune response in an additional tumor model, the LL/2 mouse syngeneic lung cancer cell line harboring $Kras^{G12C}$ and $Nras^{Q61H}$ mutations was employed (25). After deleting the *Nras* gene using CRISPR, LL/2 tumors were grown in immune-competent C57Bl/6 mice and treated with MRTX849 at 100 mg/kg every day or vehicle or 4 or 8 days and tumors were disaggregated and collected for flow cytometry. Tumors treated with MRTX849 decreased in volume over this sample collection time course (Supplementary Fig. S3A). From the myeloid cell flow cytometry analysis, M1-polarized macrophages were increased at each time point, while monocytic MDSCs were reduced at day 4 and granulocytic MDSCs were reduced at day 8 (Supplementary Fig. S3B). Furthermore, populations of T-cell origin including $CD3^+$, $CD4^+$, $CD4^+$ Th, $CD8^+$, Treg, NK, and NKT cell populations were all increased at day 4 and/or day 8 (Supplementary Fig. S3C). The alterations in immune cell populations in $Kras^{G12C}$-mutant LL/2 tumors following treatment with MRTX849 are similar to the effects observed in the CT26 $Kras^{G12C}$ model and further suggest KRAS inhibition leads to a marked reversal of the immunosuppressive program mediated by oncogenic $Kras^{G12C}$.

To further characterize T-cell populations in CT26 $Kras^{G12C}$ tumors following single-agent and combination therapy, T-cell receptor beta (TCRB) sequencing was performed on tumors from vehicle, MRTX849, anti–PD-1 antibody and combination-treated mice. A highly significant increase in T-cell frequency and diversity was observed in MRTX849 and combination-treated tumors compared with PD-1–treated or vehicle-treated tumors (Supplementary Fig. S4). An increase in T-cell frequency was also observed in PD-1 monotherapy treated tumors relative to vehicle-treated tumors. These data corroborate the increase in T-cell abundance observed by flow cytometry by MRTX849 monotherapy and in combination and demonstrate T-cell diversity was expanded accordingly. The increase in T-cell diversity is likely directly related to an increase in the number of tumor antigens recognized by the immune system following the tumor cell killing and reversal of immune suppression induced by MRTX849 treatment. Although T-cell clonality was not increased by MRTX849 or combination treatment, the dramatic increase in T-cell infiltration (frequency) and diversity provides strong evidence of a mounting adaptive cell-mediated, antitumor immune response.

### MRTX849 demonstrates acquired adaptive tumor immunity and durable complete responses in most mice treated with MRTX849 in combination with an anti–PD-1 antibody

To evaluate the ability of MRTX849 to augment the antitumor activity of anti–PD-1 therapy, CT26 *Kras*$^{G12C}$ tumor-bearing BALB/c mice were treated with an isotype control antibody, MRTX849, anti–PD-1 antibody, or the combination in a study designed to assess antitumor response and survival of tumor bearing mice (Fig. 4A and B). Treatment of CT26 *Kras*$^{G12C}$ tumor-bearing mice with an anti–PD-1 antibody demonstrated minimal tumor growth inhibition compared with isotype control treatment. Treatment with MRTX849 as a single agent resulted in rapid tumor regression, including complete responses; however, tumor regrowth despite continued treatment was observed in nine of 10 mice. In contrast, treatment with the combination of MRTX849 and the anti–PD-1 antibody also resulted in rapid regression of tumors in all mice; however, a durable complete tumor response without evidence of regrowth was observed in six of 10 mice. This translated to increased survival benefit in the combination group compared with all other groups.

To determine whether adaptive antitumor immunity was acquired in the six combination-treated mice and the one MRTX849-treated mouse that exhibited durable complete responses, CT26 *Kras*$^{G12C}$ cells were reimplanted on the opposite flank of these animals and tumors did not form in any of the mice (Fig. 4C). As a control, a cohort of treatment-naïve mice were implanted at the same time and tumors formed normally in 13 of 14 mice. These data provide clear evidence MRTX849 augmented PD-1 therapy and that the combination resulted in durable adaptive antitumor immunity.

To characterize the growth and evaluate the response to therapy in an immune compromised mouse strain, CT26 *Kras*$^{G12C}$ tumors were established in *nu/nu* mice and treated with MRTX849 at 100 mg/kg every day. Tumors also regressed following MRTX849 treatment; however, the magnitude and duration of the antitumor response was diminished compared with the complete responses observed in the same tumor model established in the BALB/c strain (Supplementary Fig. S5; Fig. 4A). These data suggest part of the mechanism of action of single-agent MRTX849 includes engagement of the adaptive immune response elicit enhanced antitumor activity.

### In *Kras*$^{G12C}$-mutant GEM lung cancer models, KRAS$^{G12C}$ inhibition reconditions the tumor immune microenvironment and anti–PD-1 combination therapy extends PFS

MRTX1257 (Supplementary Fig. S6), a close analog of MRTX849 that is similarly efficacious in selected tumor models *in vivo*, was used to evaluate the effects of KRAS$^{G12C}$ inhibition in GEM lung cancer models. Lung tumor-bearing LSL-*Kras*$^{G12C}$ *Trp53*$^{R270H}$ GEM mice were administered either vehicle plus isotype control, vehicle plus anti-mouse PD-1 antibody, MRTX1257 at 50 mg/kg every day, or MRTX1257 plus anti-mouse PD-1 for 6 days followed by tumor harvest and flow cytometry for lymphocyte and myeloid cell populations. Several CD8$^+$ T-cell populations (CD8$^+$, exhausted CD8$^+$ and CD69$^+$ activated T cells) were increased, Gr1+ MDSCs were decreased whereas granulocytic myeloid-derived suppressor cells (G-MDSC) were increased (Fig. 5A and B) following MRTX1257 treatment. Combination treatment with MRTX1257 plus an anti–PD-1 antibody led to trends that were similar compared with MRTX1257-treated tumors, whereas treatment

with an anti–PD-1 antibody resulted in little change in the $CD8^+$ T-cell populations (Fig. 5A and B) but similar changes in the MDSC populations compared with the MRTX1257 single-agent–treated tumors.

To evaluate the effect of PD-1 blockade therapy on $Kras^{G12C}$ GEMMs in combination with MRTX849, we crossed $Kras^{G12C}$ mice with a $Msh2^{tm2.1Rak}$ strain to generate $KRAS^{G12C};Msh2^{fl/fl}$ lung GEM (KCM). Tumors from this model are genomically unstable due to MSH2 loss of function and are likely more susceptible to immune checkpoint blockade due to the presence of an increased mutation/neoantigen burden (26). Treatment with either 10 mg/kg MRTX849 or MRTX849 plus anti–PD-1 resulted in tumor regression at 2 and 4 weeks (Fig. 5C; Supplementary Fig. S7). Although the tumor volume of combination-treated mice did not reach statistical significance compared to MRTX849 single-agent–treated tumors using ANOVA multiple comparisons, there was a trend of greater regression in combination-treated tumors. Moreover, PFS was significantly improved in MRTX849 plus a-PD-1 antibody–treated versus MRTX849 single-agent–treated mice (Fig. 5D). The marked alterations in the tumor immune cell composition and the increased antitumor effects of $KRAS^{G12C}$ inhibition plus anti–PD-1 therapy in GEM lung cancer models demonstrate $KRAS^{G12C}$ inhibition reverses immunosuppressive programs in KRAS-driven spontaneous tumor model systems and provide strong preclinical evidence supporting the combination of $KRAS^{G12C}$ and PD-1 inhibitors to treat $KRAS^{G12C}$-mutant cancers.

## Discussion

Understanding the mechanism of action of covalent $KRAS^{G12C}$ inhibitors represents an important step to maximize the full potential of this novel class of therapeutics. In particular, a thorough understanding of the molecular effects and immune sequelae of $KRAS^{G12C}$ inhibition in the context of CIT is of high interest. On one hand, $KRAS^{G12C}$ mutations are transversion mutations associated with smoking, a high TMB and PD-L1 positivity, each of which are factors that correlate with response to CIT. On the other hand, KRAS activation results in an immunosuppressive state related to immune evasion through decreased antigen presentation and increased expression of immunosuppressive cytokines that aid recruitment of immunosuppressive cell types. These phenomena are implicated in resistance to CIT. The observation that CIT is effective in a subset of $KRAS^{G12C}$-mutant NSCLC demonstrate evasion of the immune system via the PD-1 pathway is critical for progression of $KRAS^{G12C}$-mutant cancers, but also that further augmentation of an immune response in treatment of these cancers may be harnessed to improve treatment outcomes (4, 10, 11). These data highlight the need to better understand the pathways regulated by KRAS and PD-1 to develop strategies to improve outcomes for $KRAS^{G12C}$-mutant patients. Several mechanisms have previously been identified that demonstrate KRAS actively suppresses antitumor immunity including reduction of tumor MHC class I expression and inducing an immunosuppressive tumor microenvironment in part through regulation of VEGFA, IL8, and CXCL family cytokines (12-15, 22). By analyzing the effects of MRTX849 on immune signaling pathways in human cell line xenograft models grown in immune compromised mice, several tumor cell–centric immune effects were identified. The changes in RNA and protein levels of key immune signaling molecules shortly after MRTX849

treatment demonstrate reversal of multiple immunosuppressive programs is one of the first consequences of KRAS$^{G12C}$ inhibition *in vivo*.

The reduction of MDSC and immunosuppressive M2-polarized macrophage populations with a concomitant increase in key lymphocyte populations following treatment with single-agent MRTX849 suggests KRAS$^{G12C}$ inhibitors may trigger an antitumor immune response as a key component of their antitumor mechanism of action. Notably, these effects were observed in syngeneic mouse cancer cell line–derived lung and colon cancer tumor models as well as a GEM model of lung cancer. Each of these models are reflective of cancer types with the highest frequency of *KRAS$^{G12C}$* mutations. The diminished antitumor effect observed by MRTX849 in the tumors grown in the T-cell–deficient *nu/nu* strain further supports the hypothesis that changes in immune cell populations following KRAS inhibition contribute to the antitumor effects of the drug.

Although single-agent MRTX849 led to significant regression in immune-competent tumor models, durable complete responses were only observed with anti–PD-1 combination therapy suggesting that further enhancement of an antitumor immune response through blocking the PD-1 pathway may be critical to provide longer-lasting disease control in patients. In the CT26 *Kras$^{G12C}$* model, in addition to the reduction of granulocytic and monocytic MDSC populations, macrophage phenotypes were shifted away from an immunosuppressive M2 phenotype toward an M1-polarized phenotype. Together, these observations indicated that every intratumoral myeloid population was essentially shifted toward an immunestimulated state. These changes were likely related to and may have created a favorable microenvironment to enable an increase in major lymphocytic cell populations, including CD4$^+$ T, CD8$^+$ T, CD19$^+$ B, and NK cells. Therefore, the further enhancement of a T-cell–dependent adaptive immune response through addition of PD-1 inhibition would be predicted to induce the elimination of the remainder of antigen-positive tumor cells. The increase in Tregs may be a consequence of a productive antitumor immune response and represent a mechanism whereby the immune system limits the response. Finally, not only did cotargeting the PD-1 pathway in concert with KRAS$^{G12C}$ inhibition induce durable complete responses, the combination endowed the cured mice with durable immunity against subsequent tumor engraftment. This combination was therefore required to markedly reverse the profound immune suppression present in KRAS-mutant tumors (27).

Suppression of MHC class I by KRAS signaling may also be a key molecular feature of KRAS-mutant cancers allowing these cancers to evade the immune system and grow unchecked (22). In addition to the increased tumor antigens available for presentation following direct tumor cell killing by MRTX849, the reversal of tumor antigen suppression on tumor cells through increase of MHC protein expression coupled with the increase in dendritic cells following MRTX849 treatment likely work in concert to further expose tumor antigens previously not recognized by the immune system. Together, these factors would be predicted to facilitate an enhanced tumor cell–directed immune response. In addition, the reduction of intratumoral immunosuppressive cell populations creates a tumor microenvironment conducive to antigen presentation. Finally, the increase in T cells and T-cell diversity in the tumor provides strong evidence that an adaptive antitumor immune response is induced following MRTX849 and combination treatment.

Of note, similar immune cell changes have been observed following MEK inhibition and MEK plus PD-1 pathway inhibition supporting the role of the KRAS/MEK/ERK pathway in mediating an enhanced adaptive immune response (28). However, in contrast to MEK inhibition, treatment with a $KRAS^{G12C}$ inhibitor is poised to enable more complete inhibition of the primary oncogenic driver and is clearly advantageous compared with MEK inhibition which has been challenging to deliver to *KRAS*-mutant patients due to incomplete target inhibition and dose-limiting toxicities related to the importance of the RAS/MEK/ERK pathways in normal cells. These data also exhibit several parallels with BRAF-mutant melanoma. In this disease, BRAF mutations have been shown to induce an immune-suppressed tumor microenvironment via suppression of tumor antigen expression, secretion of immune inhibitory cytokines and the presence of immune inhibitory cells including MDSCs, tumor-associated macrophages, and Tregs (29-32). Treatment with BRAF inhibitors result in increased antigen expression, decreased expression of VEGF and immunosuppressive cytokines IL6 and IL8 and enriched T-cell infiltrates.

Our findings in the $Kras^{G12C}$-engineered CT26 model are also in agreement with a previous study exploring the pharmacodynamic and antitumor effects of the $KRAS^{G12C}$ inhibitor AMG510 alone and in combination with anti–PD-1 therapy (1). The current studies extend these data and also demonstrate that $KRAS^{G12C}$ regulates tumor cell immune signaling, antigen presentation, and additional microenvironmental factors. Moreover, the dramatic reconditioning of the tumor immune microenvironment was also observed in additional models including a second syngeneic mouse model and autochthonous GEM model. Together, these findings provide compelling evidence that $KRAS^{G12C}$ inhibition induces proimmunogenic effects in multiple tumor contexts.

Although targeted therapies directed at oncogenic drivers in NSCLC are highly effective in a majority of patients, unfortunately, disease progression invariably occurs for most patients. Conversely, anti–PD-1–based therapies are not effective for most patients as a single agent; however, in patients that do respond, responses are notable for their durability. The combination of a $KRAS^{G12C}$-targeted therapy with CIT may potentially bring the best of both therapeutic classes together—a high response rate consistent with oncogene-targeted therapies in NSCLC coupled with the durable clinical benefit observed with CIT. The high TMB and PD-L1 expression and responsiveness to CIT for *KRAS*-mutant NSCLC also contrasts with observations in *EGFR, ALK, ROS1*, and *RET* alteration positive cancers suggesting a unique opportunity to combine a targeted therapy and CIT in this oncogene-driven NSCLC segment (33, 34). Ultimately, therefore, this combination may provide a therapeutic strategy that provides increasingly durable clinical benefit for a large proportion of patients with $KRAS^{G12C}$-mutant NSCLC.

## Supplementary Material

Refer to Web version on PubMed Central for supplementary material.

## Acknowledgments

K.-K. Wong received research funding from Mirati Therapeutics. We thank Molecular Diagnostic Services (MDS) for mouse pharmacology support, MI Bioresearch for flow cytometry support, Adaptive Biotechnologies for TCRB sequencing, and Flagship Biosciences for IHC support.

## References

1. Canon J, Rex K, Saiki AY, Mohr C, Cooke K, Bagal D, et al.The clinical KRAS (G12C) inhibitor AMG 510 drives anti-tumour immunity. Nature2019;575: 217–23. [PubMed: 31666701]
2. Hallin J, Engstrom LD, Hargis L, Calinisan A, Aranda R, Briere DM, et al.The KRAS(G12C) inhibitor MRTX849 provides insight toward therapeutic susceptibility of KRAS-mutant cancers in mouse models and patients. Cancer Discov2020;10:54–71. [PubMed: 31658955]
3. Martinez P, Peters S, Stammers T, Soria J-C. Immunotherapy for the first-line treatment of patients with metastatic non-small cell lung cancer. Clin Cancer Res2019;25:2691–8. [PubMed: 30642913]
4. Borghaei H, Paz-Ares L, Horn L, Spigel DR, Steins M, Ready NE, et al.Nivolumab versus docetaxel in advanced nonsquamous non-small-cell lung cancer. N Engl J Med2015;373:1627–39. [PubMed: 26412456]
5. Garon EB, Rizvi NA, Hui R, Leighl N, Balmanoukian AS, Eder JP, et al.Pembrolizumab for the treatment of non-small-cell lung cancer. N Engl J Med2015;372:2018–28. [PubMed: 25891174]
6. Gandhi L, Rodríguez-Abreu D, Gadgeel S, Esteban E, Felip E, De Angelis F, et al.Pembrolizumab plus chemotherapy in metastatic non-small-cell lung cancer. N Engl J Med2018;378:2078–92. [PubMed: 29658856]
7. Dogan S, Shen R, Ang DC, Johnson ML, D'Angelo SP, Paik PK, et al.Molecular epidemiology of EGFR and KRAS mutations in 3,026 lung adenocarcinomas: higher susceptibility of women to smoking-related KRAS-mutant cancers. Clin Cancer Res2012;18:6169–77. [PubMed: 23014527]
8. Gandara DR, Paul SM, Kowanetz M, Schleifman E, Zou W, Li Y, et al.Blood-based tumor mutational burden as a predictor of clinical benefit in non-small-cell lung cancer patients treated with atezolizumab. Nat Med2018;24:1441–8. [PubMed: 30082870]
9. Coelho MA, de Carné Trécesson S, Rana S, Zecchin D, Moore C, Molina-Arcas M, et al.Oncogenic RAS signaling promotes tumor immunoresistance by stabilizing PD-L1 mRNA. Immunity2017;47:1083–99. [PubMed: 29246442]
10. Jeanson A, Tomasini P, Souquet-Bressand M, Brandone N, Boucekine M, Grangeon M, et al.Efficacy of immune checkpoint inhibitors in KRAS-mutant non-small cell lung cancer (NSCLC). J Thorac Oncol2019;14: 1095–101. [PubMed: 30738221]
11. Passiglia F, Cappuzzo F, Alabiso O, Bettini AC, Bidoli P, Chiari R, et al.Efficacy of nivolumab in pre-treated non-small-cell lung cancer patients harbouring KRAS mutations. Br J Cancer2019;120:57–62. [PubMed: 30377342]
12. Kortlever RM, Sodir NM, Wilson CH, Burkhart DL, Pellegrinet L, Brown Swigart L, et al.Myc cooperates with Ras by programming inflammation and immune suppression. Cell2017;171:1301–15. [PubMed: 29195074]
13. Liao W, Overman MJ, Boutin AT, Shang X, Zhao Di, Dey P, et al.KRAS-IRF2 axis drives immune suppression and immune therapy resistance in colorectal cancer. Cancer Cell2019;35:559–72. [PubMed: 30905761]
14. Okada F, Rak JW, Croix BS, Lieubeau B, Kaya M, Roncari L, et al.Impact of oncogenes in tumor angiogenesis: mutant K-ras up-regulation of vascular endothelial growth factor/vascular permeability factor is necessary, but not sufficient for tumorigenicity of human colorectal carcinoma cells. Proc Natl Acad Sci U S A1998;95:3609–14. [PubMed: 9520413]
15. Rak J, Mitsuhashi Y, Bayko L, Filmus J, Shirasawa S, Sasazuki T, et al.Mutant ras oncogenes upregulate VEGF/VPF expression: implications for induction and inhibition of tumor angiogenesis. Cancer Res1995;55:4575–80. [PubMed: 7553632]
16. Rak J, Mitsuhashi Y, Sheehan C, Tamir A, Viloria-Petit A, Filmus J, et al.Oncogenes and tumor angiogenesis: differential modes of vascular endothelial growth factor up-regulation in ras-transformed epithelial cells and fibroblasts. Cancer Res2000;60:490–8. [PubMed: 10667605]

17. Terme M, Pernot S, Marcheteau E, Sandoval F, Benhamouda N, Colussi O, et al.VEGFA-VEGFR pathway blockade inhibits tumor-induced regulatory T-cell proliferation in colorectal cancer. Cancer Res2013;73:539–49. [PubMed: 23108136]
18. Voron T, Marcheteau E, Pernot S, Colussi O, Tartour E, Taieb J,et al.Control of the immune response by pro-angiogenic factors. Front Oncol2014;4:70. [PubMed: 24765614]
19. Socinski MA, Jotte RM, Cappuzzo F, Orlandi F, Stroyakovskiy D, Nogami N, et al.Atezolizumab for first-line treatment of metastatic nonsquamous NSCLC. N Engl J Med2018;378:2288–301. [PubMed: 29863955]
20. Ancrile BB, O'Hayer KM, Counter CM. Oncogenic ras-induced expression of cytokines: a new target of anti-cancer therapeutics. Mol Interv2008;8:22–7. [PubMed: 18332481]
21. Sunaga N, Imai H, Shimizu K, Shames DS, Kakegawa S, Girard L, et al.Oncogenic KRAS-induced interleukin-8 overexpression promotes cell growth and migration and contributes to aggressive phenotypes of non-small cell lung cancer. Int J Cancer2012;130:1733–44. [PubMed: 21544811]
22. El-Jawhari JJ, El-Sherbiny YM, Scott GB, Morgan RSM, Prestwich R, Bowles PA, et al.Blocking oncogenic RAS enhances tumour cell surface MHC class I expression but does not alter susceptibility to cytotoxic lymphocytes. Mol Immunol2014;58:160–8. [PubMed: 24365750]
23. Castle JC, Loewer M, Boegel S, de Graaf J, Bender C, Tadmor AD, et al.Immunomic, genomic and transcriptomic characterization of CT26 colorectal carcinoma. BMC Genomics2014;15:190. [PubMed: 24621249]
24. Baldelli E, Bellezza G, Haura EB, Crinó L, Cress WD, Deng J, et al.Functional signaling pathway analysis of lung adenocarcinomas identifies novel therapeutic targets for KRAS mutant tumors. Oncotarget2015;6:32368–79. [PubMed: 26468985]
25. Giannou AD, Marazioti A, Kanellakis NI, Giopanou I, Lilis I, Zazara DE, et al.NRAS destines tumor cells to the lungs. EMBO Mol Med2017;9:672–86. [PubMed: 28341702]
26. Downey CM, Jirik FR. DNA mismatch repair deficiency accelerates lung neoplasm development in K-ras(LA1/+) mice: a brief report. Cancer Med2015;4:897–902. [PubMed: 25773971]
27. Chen DS, Mellman I. Oncology meets immunology: the cancer-immunity cycle. Immunity2013;39:1–10. [PubMed: 23890059]
28. Loi S, Dushyanthen S, Beavis PA, Salgado R, Denkert C, Savas P, et al.RAS/MAPK activation is associated with reduced tumor-infiltrating lymphocytes in triple-negative breast cancer: therapeutic cooperation between MEK and PD-1/PD-L1 immune checkpoint inhibitors. Clin Cancer Res2016;22:1499–509. [PubMed: 26515496]
29. Mandalà M, De Logu F, Merelli B, Nassini R, Massi D. Immunomodulating property of MAPK inhibitors: from translational knowledge to clinical implementation. Lab Invest2017;97:166–75. [PubMed: 27991907]
30. Frederick DT, Piris A, Cogdill AP, Cooper ZA, Lezcano C, Ferrone CR, et al.BRAF inhibition is associated with enhanced melanoma antigen expression and a more favorable tumor microenvironment in patients with metastatic melanoma. Clin Cancer Res2013;19:1225–31. [PubMed: 23307859]
31. Wilmott JS, Long GV, Howle JR, Haydu LE, Sharma RN, Thompson JF, et al.Selective BRAF inhibitors induce marked T-cell infiltration into human metastatic melanoma. Clin Cancer Res2012;18:1386–94. [PubMed: 22156613]
32. Sumimoto H, Imabayashi F, Iwata T, Kawakami Y. The BRAF-MAPK signaling pathway is essential for cancer-immune evasion in human melanoma cells. J Exp Med2006;203:1651–6. [PubMed: 16801397]
33. Dong Z-Yi, Zhong W-Z, Zhang Xu-C, Su J, Xie Z, Liu Si-Y, et al.Potential predictive value of TP53 and KRAS mutation status for response to PD-1 blockade immunotherapy in lung adenocarcinoma. Clin Cancer Res2017;23:3012–24. [PubMed: 28039262]
34. Scheel AH, Ansén S, Schultheis AM, Scheffler M, Fischer RN, Michels S, et al.PD-L1 expression in non-small cell lung cancer: correlations with genetic alterations. Oncoimmunology2016;5:e1131379. [PubMed: 27467949]

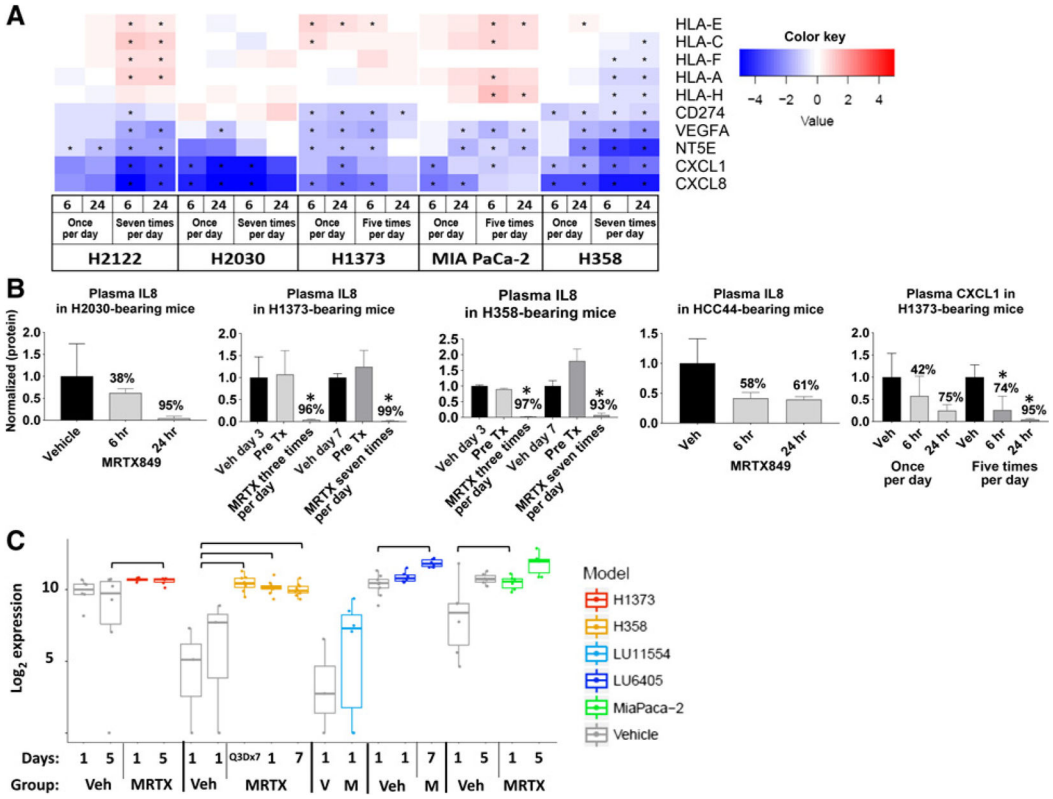


**Figure 1.**

$KRAS^{G12C}$ regulates antigen presentation and an immunosuppressive tumor microenvironment in a tumor cell–intrinsic manner. **A,** Heatmap of $\log_2$ fold changes in RNA expression from RNA-seq data of selected immune-modulating genes in human tumor xenografts established in immune-compromised mice dosed orally with MRTX849 once every day, five times per day or seven times per day and harvested 6 or 24 hours after administration relative to expression in vehicle-treated tumors. "*" indicates FDR < 0.05, $n = 3$ per treatment group. **B,** Plasma concentration of selected secreted immune-modulating proteins in immune-compromised mice harboring human tumor xenografts orally administered vehicle or MRTX849 every day or for the number of days indicated. Plasma was collected 24 hours after last dose for the H1373 and H358 models and as indicated for other models. "*" indicates Student $t$ test, $P = 0.05$, MRTX849-treated plasma compared with vehicle-treated plasma, $n = 3$ per treatment group. Veh = vehicle; Pre Tx = pretreatment. **C,** $\log_2$ expression of human MHC class I protein in human xenograft models established in immune-compromisedmice orallyadministered vehicle or 100 mg/kg MRTX849 once every day, five times per day or seven times per day. Presence of a bar indicates statistically significant difference between indicated groups by Student $t$ test, $P < 0.05$, $n = 3$ per treatment group. Two different vehicle-treated tumor volume groups (300 and 500 $mm^3$) were used for the H358 study.

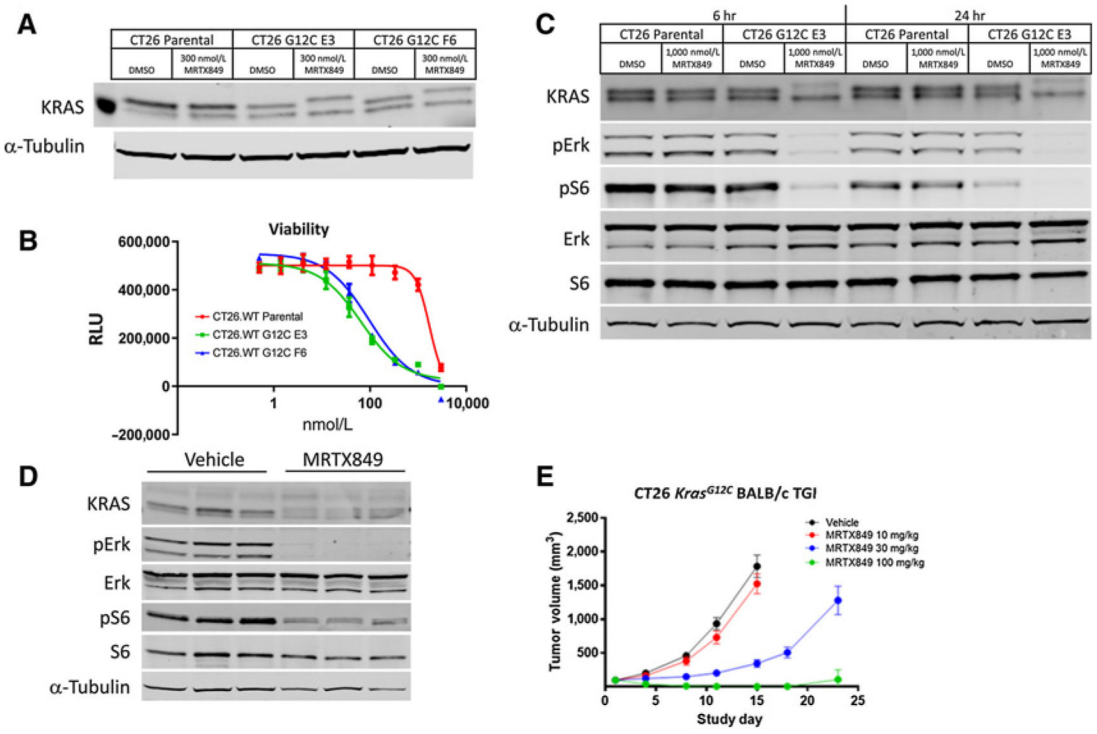


**Figure 2.**

CRISPR/Cas9-engineered CT26 *Kras*$^{G12C}$ cells and tumors are sensitive to MRTX849 treatment. **A,** Parental CT26.WT and G12C-engineered CT26.WT cell lines (CT26 *Kras*$^{G12C}$) derived from single-cell clones (clone E3 and F6) were incubated with 300 nmol/L of MRTX849 for 24 hours and probed via immunoblot with total anti-KRAS and anti-α-tubulin antibodies. The increased molecular weight of KRAS$^{G12C}$ in the MRTX849-treated lane is indicative of covalent KRAS$^{G12C}$ modification. The molecular weight of the standard protein to the left of the DMSO-treated parental lysate is 20 kD. **B,** A Cell Titer-Glo viability assay was performed on parental and CT26 *Kras*$^{G12C}$ E3 and F6 cell line clones treated with MRTX849 *in vitro* for 3 days. **C,** Parental CT26.WT and CT26 *Kras*$^{G12C}$ clone E3 cells were incubated with 1,000 nmol/L of MRTX849 for 6 or 24 hours and lysates were probed via immunoblot with anti-KRAS, pERK (Thr202/Tyr204), ERK, pS6 (Ser235/236), S6 or α-tubulin. **D,** 100 mg/kg MRTX849 was administered orally to mice bearing CT26 *Kras*$^{G12C}$ E3 tumors. Tumors were harvested 6 hours after dosing and lysates were probed via immunoblot with anti-KRAS, pERK (Thr202/Tyr204), ERK, pS6 (Ser235/236), S6 or α-tubulin. **E,** 10, 30, and 100 mg/kg MRTX849 was administered orally every day to BALB/cmice bearing established CT26 *Kras*$^{G12C}$ tumors ($n$ = 7 per treatment group; average starting tumor volume ~100mm$^3$) and tumor volume was measured over the study at indicated days. Average tumor volume ± SEM shown.

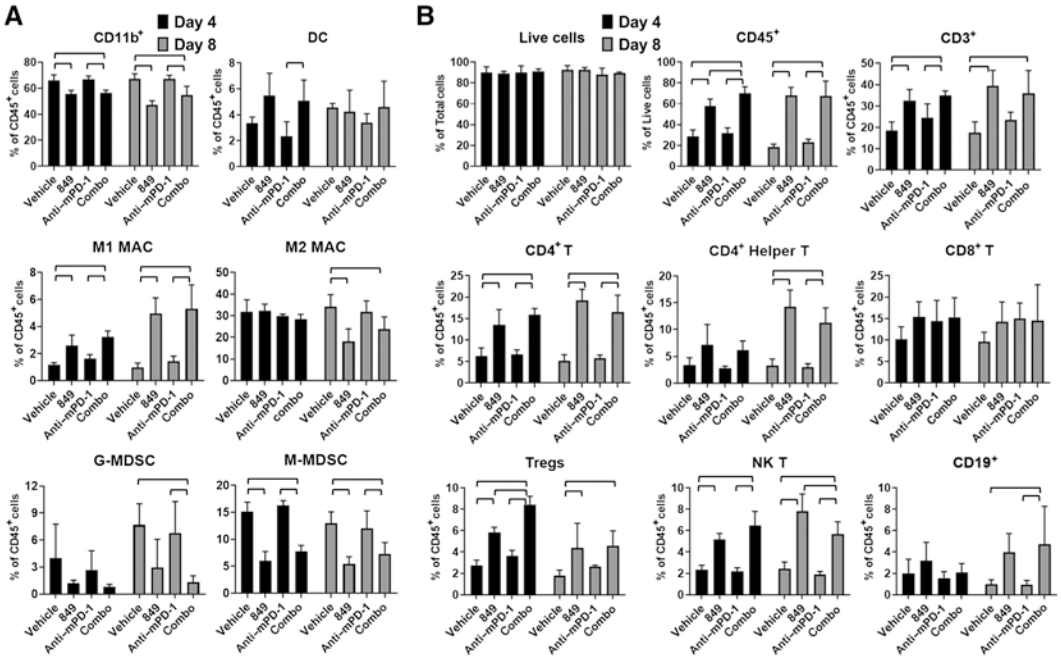


**Figure 3.**

MRTX849 and combined MRTX849 and anti–PD-1 administration markedly alters immune cell populations in the tumor microenvironment. MRTX849 (100 mg/kg), rat IgG2a isotype Control antibody (10 mg/kg, Bio X cell lot No. 686318F1B), and mouse PD-1 antibody at 10 mg/kg (Bio X cell clone 29F.1A12) were administered orally, daily (MRTX849) or intraperitoneally, every 3 days (PD-1 and isotype control) or in combination to mice bearing established, subcutaneous CT26 $Kras^{G12C}$ tumors ($n = 4$ per treatment group; average starting tumor volume approximately 220 $mm^3$ (vehicle and PD-1–treated cohorts) or approximately 730 $mm_3$ (MRTX849 or combination-treated cohorts. Intratumoral myeloid (**A**) and lymphoid (**B**) populations were analyzed in excised disaggregated tumors by flow cytometry following 4 or 8 days of treatment administration. Analyzed cell populations include DC—dendritic cell, M1MAC—M1-polarized macrophage, M2MAC—M2-polarized macrophage, G-MDSC—granulocytic myeloid-derived suppressor cell, M-MDSC—monocytic MDSC, Tregs—T regulatory cells, NK T—natural killer T cells denoted by cell lineage–specific markers including CD11b, CD45, CD3, CD4, CD8, etc. (see Supplementary Methods). Flow cytometry analysis on single-cell suspensions of CT26 $KRAS^{G12C}$ tumors treated with vehicle or MRTX849 was run twice and data were similar between experiments. Bars denotes statistical significance by one-way ANOVA with *post hoc* Tukey test.

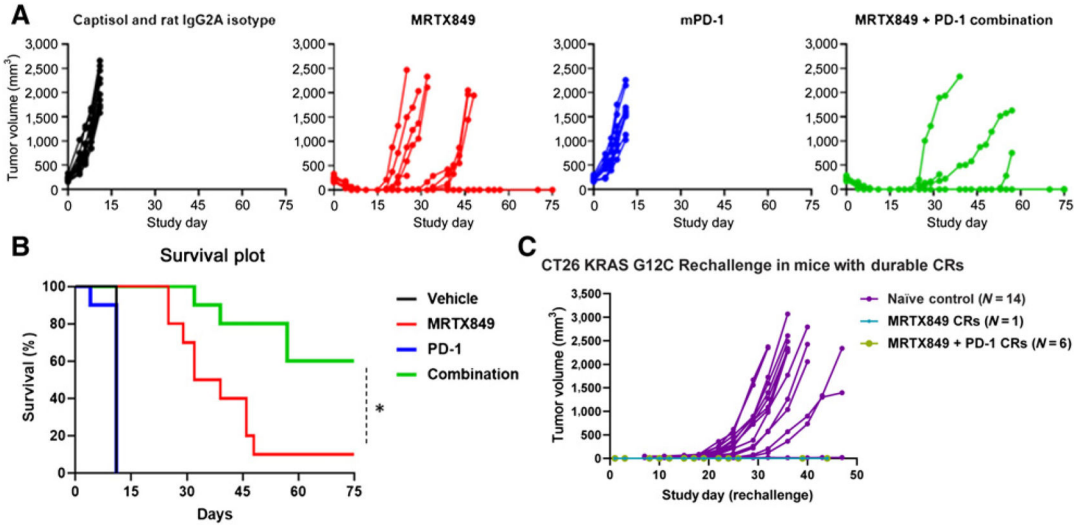


**Figure 4.**

MRTX849 and anti–PD-1 combination treatment leads to durable complete responses in the majority of treated mice. **A,** MRTX849 (100 mg/kg), rat IgG2a isotype control antibody (10 mg/kg, Bio X cell lot No. 686318F1B), and mouse PD-1 antibody (10 mg/kg, Bio X cell clone 29F.1A12) were administered orally, daily (MRTX849) and intraperitoneally, every 3 days × three doses (PD-1 and isotype control) alone or in combination as denoted to mice bearing established, subcutaneous CT26 $Kras^{G12C}$ tumors on the right flank ($n$ = 10/treatment group, average starting tumor volume of ~220 $mm^3$). Vehicle was dosed through study day 10, MRTX849 was dosed through study day 25 and PD-1 was dosed on study days 1, 4, and 7. Data are illustrated as individual tumor volumes over the measured time course for the efficacy and rechallenge studies. **B,** Survival in the combination-treated cohort was statistically significant compared with all other treatment cohorts by the Mantel-Cox test. "*" denotes adjusted $P < 0.05$. **C,** Data in the rechallenge graph depict individual tumor volumes from reimplantation of 1e6 CT26 $Kras^{G12C}$ cells into the left flank in the one MRTX849-treated mouse and the six combination-treated mice each of which exhibited durable complete tumor responses (CR) in the first implant/study (**A**). A cohort of naïve mice were also implanted as a control and tumors developed normally in 13 of 14 mice (denoted in purple).

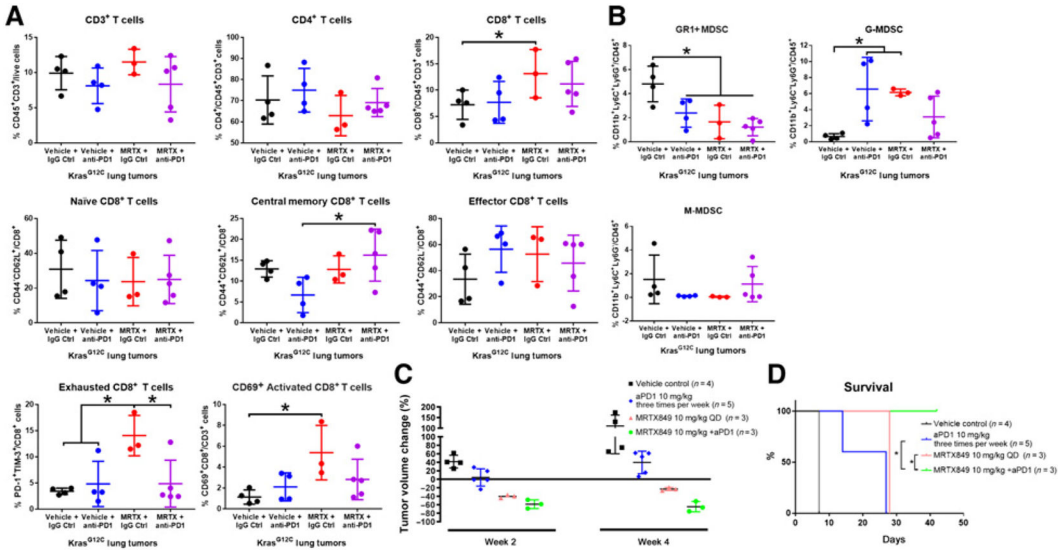


**Figure 5.**

MRTX1257 reconditions the tumor immune microenvironment and MRTX849 plus anti–PD-1 therapy prolongs survival in *Kras*$^{G12C}$-mutant GEMMs. **A** and **B,** Lung tumor-bearing LSL-*Kras*$^{G12C}$ *Trp53*$^{R270H}$ GEM mice were administered vehicle plus isotype control, vehicle plus anti-mouse PD-1 antibody (10 mg/kg three times per week, Bio X cell clone 29F.1A12), MRTX1257 (50 mg/kg) or MRTX1257 plus anti-mouse PD-1 for 6 days. Mice were euthanized on day 7 and lung tumor nodules were harvested and disaggregated for immune profiling for lymphoid (**A**) or myeloid (**B**) populations by flow cytometry. Flow cytometry data are expressed for individual tumors using scatter plots along with mean ± SD for selected cell markers as defined in the Supplementary Materials and Methods. **C,** Tumor volume was monitored in repeat dose efficacy studies in the LSL-*Kras*$^{G12C}$ *Msh2*$^{fl/f}$ lung GEM model at baseline and at week 2 and week 4. See Supplementary Fig. S7 for statistical analysis. **D,** PFS analysis demonstrates combination treatment led to a statistically significant improvement in survival compare with MRTX849 or anti–PD-1 single-agent treatment using the log-rank (Mantel-Cox) test ($P < 0.05$).